

Conformational changes in the AdeB transmembrane efflux pump by amphiphilic peptide Mastoparan-B, down-regulates expression of the *adeB* gene and restores antibiotics susceptibility

Mohammad Reza Shakibaie¹, Farzan Modaresi², Omid Azizi³, Omid Tadjrobehkar¹, and Mohammad Mehdi Ghaemi¹

¹Kerman University of Medical Sciences

²Jahrom University of Medical Science

³Torbat Heydarieh University of Medical Sciences

December 20, 2022

Abstract

No report exists on the role of Mastoparan B (MP-B) as an RND efflux pump inhibitor in multi-drug resistant (MDR) *Acinetobacter baumannii*. Here, we performed a series of in-silico experiments to predict the inhibition of the AdeB efflux pump by MP-B as a drug target agent. For this reason, an MDR strain of *A. baumannii* was subjected to minimum inhibitory concentration (MIC) against 12 antibiotics as well as MP-B. Expression of the *adeB* gene in the absence and presence of sub-MIC of MP-B was studied by qRT-PCR. It was found that MP-B had potent antimicrobial activity (MIC=1 μ g/ml) associated with a 20-fold decrease in its expression at sub-MIC of MP-B. The stereochemical analysis using several automated servers confirmed that the AdeB is an inner membrane of the RND tripartite complex system with helix-turn-helix conformation and a pore rich in Phe, Ala, and Lys residue. The best model that showed high accuracy ($Z=1.2$, $C=1.41$, $TM=0.99$, and $RMSD=4.4$) was selected for docking purposes using the Site Map tool, and the correct protein-peptide complexes were simulated in the BioLiP platform. The molecular docking via AutoDock/Vina suggested that MP-B form H-bound with amino acid residues of the AdeB helix-5 and caused a shift in the dihedral angle by distances of 9.0 Å, 9.3 Å, and 9.6 Å, respectively. This shift was detected by the AlphaFold 2 tool and influenced the overall druggability of the protein. From the results, we concluded that, MP-B can be a good candidate for inhibition of bacterial efflux pump.



1 INTRODUCTION

Computation chemistry has greatly increased our knowledge about protein conformation and drug interaction and helped us better understand microbial infection treatment.¹ Biomolecular simulation with models allows for investigations of target proteins' structure and function features, which are useful for identifying drug-binding sites and elucidating drug action mechanisms.^{2,3} Recently a breakthrough in the 3D construction of various proteins occurred with the invention of the AlphaFold Protein Structure Database in cooperation with EMBL-EBI. AlphaFold can accurately predict 3D models of protein structures and is accelerating research in nearly every field of biology such as drug–target interaction.⁴

In this regard, *A. baumannii* is a Gram-negative hospital-acquired pathogen to blame for high morbidity and mortality within the medical care units such as ICUs of various hospitals across the world.⁵ Following the increasing emergence of strains that are not susceptible to any clinically used antibiotics, the WHO has ranked carbapenem-resistant strains of this bacterium in first place in its global priority pathogen list.⁶ *A. baumannii* has different resistance mechanisms against antimicrobial agents such as β -Lactam inactivation, biofilm formation, efflux pumps, alterations of the affinity for antibiotics, etc.⁷⁻⁹ One of the most important mechanism of resistance to antibiotics is the efflux pump which plays a key role in the intrinsic resistance to several antibiotics.^{10,11} The efflux pumps are divided into five superfamilies: ATP-binding cassette (ABC), small multi-drug resistance (SMR), multi-antimicrobial extrusion (MATE), major facilitator (MFS), and resistance/nodulation/division (RND).¹² The best-characterized multi-drug efflux system in *A. baumannii* is the RND superfamily.¹³ These tripartite complexes comprise an inner membrane that acts as a secondary active H^+ /drug antiporter (AdeB), extruding a vast spectrum of structurally unrelated drugs through a periplasmic membrane fusion protein channel (AdeA), connected to an outer membrane funnel shape channel

(AdeC).¹⁴ The primary RND efflux pump of *A. baumannii* (AdeABC) was first described in MDR strain BM4454.¹⁴ The *Ade* abc locus has consisted of three tandemly linked genes encoding AdeA, AdeB, and AdeC proteins and showed resistance to several antibiotic classes such as aminoglycosides, tetracyclines, and fluoroquinolones, respectively.¹⁵ The AdeB is an inner membrane protein and transports various drugs through the central pore.¹⁶ The pore is opened to the periplasm via three vestibules located at subunit interfaces and a central cavity.¹⁷ More researchers demonstrated that, the *ade* B is the most important gene in the adeABC efflux system.^{17,18} Genetic studies suggested that discrimination between the substrates in *A. baumannii* occurs mainly within the periplasmic region instead of the transmembrane region.¹⁹ Cryo-Electron Microscopy (CEM) of the monomers of the inner membrane protein suggested that AdeB can adopt three different states: access (loose), binding (tight), and extrude (release) to provide essential dynamics for the efflux process.²⁰ The AdeB trimer primarily adopts mainly a resting state (absence of antibiotics) with all promoters in a conformation devoid of transport channels or antibiotic binding sites.²¹

Transmembrane proteins are relevant for drug development since they make up more than 50% of all human drug targets given that approximately 25% of all the proteins.²² Membrane proteins are difficult to study due to their partially hydrophobic surfaces, flexibility, and lack of stability.²¹ Consequently creates the need for bioinformatics tools that can accurately identify these types of proteins by predicting their topology, position, and orientation as well as their N-terminal utilizing the contact map with coevolutionary precision matrices.²³ Several methods have been developed over the last decades that predict protein topology with high accuracy. Many of these methods are freely available as web servers, both individually or combine with several other bioinformatics tools.²⁴

In the past 20 years, scientists were unable to produce effective antibiotics against Gram-positive or Gram-negative pathogens. Furthermore, the use of nanoparticles, gene therapy, phage therapy, and immunotherapy are either costly or still in their infancy.²⁵ In contrast, the amphiphilic antimicrobial peptides like Mastoparan B (a cationic, tetradeca peptide LKLKSIVSWAKKVL-CONH₂ isolated from the venom of the hornet *Vespa basalis*) at low concentrations has potent antimicrobial activity and can be used along with antibiotics for treatment of various diseases.²⁶ These compounds frequently destabilize biological membranes by dual amphiphilic activity resulting in membrane perforation.²⁷ In recent years, numerous efflux pump inhibitors have been discovered and tested, including natural products, antibiotics, and synthetic molecules.²⁸ The combination of antibiotics with natural products circumvents the resistance phenomenon and consequently decreases the dose and drug side effects. The activity of these peptides in the combination with antibiotics on *Escherichia coli* AcrAB-TolC and the *Pseudomonas aeruginosa* MexAB-OprM complexes were well delineated.²⁹ In contrast, there is no information about the effect of Mastoparan-B on the RND efflux in *A. baumannii*. It has been reported that the phenylalanine-arginine β -naphthylamide (PA β N) a broad-spectrum efflux pump inhibitor interacts with AdeB strongly through the distal binding pocket.³⁰ In another investigation, computational screening suggested that Strictamin (Akuammilan-17-oic acid methyl ester from *Alstonia scholaris*) and Limonin (7, 16-dioxo-7, 16-dideoxylimondiol from *Citrus* spp.) exhibited binding to RND efflux pump in MDR strains of *A. baumannii*.³¹

Therefore, in the present study, for the first time, we are reporting transcriptional analysis of the *ade* B gene in the presence of Mastoparan-B, the detailed stereochemical structure of AdeB protein before and after binding to this peptide, superfamily analysis by CATH database, Gene Ontology, molecular docking, prediction of structure conformation and helix folding by AlphaFold Protein Structure Database (AlphaFold 2). The emerging picture using this peptide in combination with antibiotics further suggests opportunities for drug designs.

2 MATERIALS AND METHODS

2.1 Bacterial source and PCR-Sequencing

An MDR strain of *A. baumannii* was isolated from the previous collection³² and used for the detection of the *ade* B gene by polymerase chain reaction (PCR) technique. Briefly, total genomic DNA was extracted by a DNA genomic extraction kit (ParsTous, Iran). The amplification was carried out using

a common PCR core mixture (total volume, 50 μ l) containing 20 μ L PCR buffer, 10 μ L of 200 mM each dNTP (Bioneer, South Korea), 1 U of AmpliTaq DNA polymerase (ParsTous, Iran), 20 pmol of the forward -5' TTAACGATAGCGTTGTAACC -3' and reverse 5'- TGAGCAGACAATGGAATAGT -3' primer pair (Bioneer, Korea) and 50 ng of the genomic DNA as the PCR template. The *ade B* gene was further purified by a DNA purification kit (ParsTous, Iran) and sequenced in both directions by Sanger's dideoxy chain termination method using ABI Prism 373 DNA Sequencer (Applied Biosystems 373/3730XL, Bioneer, Korea). The *ade B* sequence was then submitted to the GenBank NCBI database (<https://www.ncbi.nlm.nih.gov/genbank/submit/>) for accession number. The BLAST program was used to find the amino acid sequence of the AdeB protein.

2. 2 Susceptibility to antibiotics and Mastoparan-B

The susceptibility of the selected strain to 12 antibiotics was carried out by disc diffusion assay and MIC methods using broth microdilution test by the Clinical and Laboratory Standards Institute (CLSI 2019) protocol.³³ At the same time, the susceptibility of the isolate to Mastoparan-B was performed by microdilution method using the Tryptic Soy broth medium, and criteria for sensitivity or resistance were measured based on our previous report.³⁴ Similarly, we performed MICs of antibiotics in the presence of sub-MIC concentration (0.5 μ g/mL) of MP-B to see any synergism between peptide and antibiotics. Before the experiment, we checked the viability of the cells at this concentration, by removing 1 ml aliquots of each sample grown in the presence and absence of 0.5 ml of MP-B at each 2 h and reading the turbidity with a UV/Vis spectrophotometer (Persia Med, AE-S60-4U) at an optical density (OD) of 600 nm. The standard cultures of *E. coli* ATTC25922 and *A. baumannii* ATCC 19606 were used as the quality control strains. All antibiotics were purchased from MAST Company, Manchester, UK. Mastoparan-B powder with 99.5% purity was purchased from Shimi-Daru (Tehran, Iran) and used as described by the manufacturer.

2. 3 Expressional analyses of the *ade B* Gene

RNA extraction, C-DNA synthesis, and relative quantitative real-time PCR (qRT-PCR) were performed to assess the expression of the *ade B* gene in the presence and absence of 0.5 μ g/ml of MP-B as described previously.³² Briefly, amplification was done using 25 μ l of SYBR®Green dye and 2 \times Real-Time PCR master mix solution (BIO FACT, Korea), followed by the addition of 1 μ l of *ade B* primer pair F: 5'- AACGGACGACCATCTTTGAGTATT-3' and R: 5- 'CAGTTGTTCCATTTTCACGCATT-3' and 5 μ l of cDNA template. Quantification of the *ade B* gene was performed by using the ABI Step One qRT-PCR system (Applied Biosystems, Foster City, CA, USA). The gene expression was calculated as a fold change (RQ) between the target gene and matched reference 16SrRNA levels based on the following formula $RQ = 2^{\Delta\Delta Ct}$. Where ΔCt is equal to the difference between the cutting point (Ct) value for the analyzed gene and Ct for the 16SrRNA reference gene as described by Livak et al.³⁵ *A. baumannii* ATCC 19660 was used as the internal control strain. Differences were assessed by Student's t-test for consideration as statistically significant.

2. 4 Classification, physicochemical parameters, and Gene Ontology

The hierarchical classification of AdeB protein to the superfamily, homologous family, predicting domains, and important functional sites were carried out by the InterPro software suite (<https://www.ebi.ac.uk/interpro/>). To classify proteins in this way, InterPro uses predictive models, known as signatures provided by several different alignments and produces a comprehensive resource for protein classification (<https://www.ebi.ac.uk/interpro/search/sequence/>). Any alignment with a TM-score [?]0.5, which is the cutoff value for a significant structural match, was used as a potential template for the target protein-peptide interaction. Furthermore, molecular weight, theoretical pI, amino acid composition, atomic composition, extinction coefficient, estimated half-life, instability index, aliphatic index, and grand average of hydropathicity (GRAVY) were computed by information stored in the Swiss-Port ProtParam database (<https://web.expasy.org/protparam/>). Gene Ontology at molecular and cellular functions was determined using the UniProtKB platform (<https://www.uniprot.org/>). We also worked on the domain-based method for the AdeB protein sequence versus structural diversity and prediction of the functional site

that exploits functional sub-classification of the superfamilies by the CATH protein classification database (<https://www.cathdb.info/>).

2. 5 Construction of phylogenetic tree of the AdeB protein

The phylogenetic tree of the AdeB protein was constructed using maximum likelihood sequence alignment Clustral Omega version 7 in the UniProtKB pipeline, and variable sites were removed by the stringent settings.³⁶ A bootstrapped was generated with RAxML (Randomized Accelerated Maximum Likelihood) version 7.0.3 with the confidence levels (%) generated from 1000 bootstrap trials.³⁶ Moreover, we choose a consensus sequence manually using similar protein sequences from the UniProtKB restricted to the *A. baumannii* AdeB protein.

2. 6 Protein dynamic simulation

From the primary amino acid sequence, the 3D model of AdeB protein was generated by the SWISS-Expasy (<https://swissmodel.expasy.org>), and I-TESSAR (<https://zhanggroup.org/I-TASSER/>) platforms using the homology modeling program. For each target, I-TASSER simulation generates a large ensemble of structural conformations, called decoys. To select the final models, I-TASSER uses the SPICKER program to cluster all the decoys based on the pair-wise structural similarity and reports up the top five models which correspond to the five closest structure clusters. The confidence of each model is quantitatively measured by the C-score that is calculated based on the significance of threading template alignments and the convergence parameters of the structure assembly simulations. Furthermore, for the evaluation of multiple, amino acids alignments and similarity matrix, we used the FASTA format of the targeted amino acids sequence and blasted in the UniProtKB database (<https://www.uniprot.org/>). The functional domains of the AdeB protein were bolded using the ROSETTA prediction tool (<https://www.rosettacommons.org/>) and the Hidden Markov Model program (HMMs) (<https://www.ebi.ac.uk/Tools/hmmer/>). The quality of obtained models was validated with a comprehensive scoring function for model quality assessment servers such as ProSA and QMEAN.^{38, 39} The dihedral angles including phi (φ) and psi (ψ) and backbone conformation were assessed using the PROCHECK tool at the PDB Sum server (<https://www.ebi.ac.uk/thornton-srv/software/PROCHECK/>). In the field of drug discovery, the use of 3D models can provide an understanding of why a certain drug compound is an inhibitor, while a related compound is not, or why certain proteins are druggable while others are not. Recently, the AlphaFold DB database resolves this problem and showed folding of protein plays a role in the druggability of targeted protein. In this study, we evaluated the accuracy of the AdeB protein structure, folding patterns of the helices and domain side chains including the interior side of the AdeB by the AlphaFold 2 database (<https://alphafold.ebi.ac.uk>). In addition, we computed the backbone dihedral angles (F) to investigate rotameric conformational for the amino acid residues binding with ligand base on the Ramachandran plot and two other model simulation apo and ligands.⁴⁰

2. 7 Prediction of the protein-peptide interaction site

Because of peptide flexibility and the transient nature of protein-peptide interactions, peptides are difficult to study experimentally. Therefore, we used computational methods for predicting structural information about protein-peptide interactions by the InterPep server (<http://wallnerlab.org/InterPep/>). The InterPep software is a powerful tool for identifying peptide-binding sites with a precision of 80% at a recall, of 20%. It is an excellent starting point for docking protocols or experiments investigating peptide interactions.

2. 8. Ligand preparation and molecular docking

Mastoparan-B with MF: C78H138N20O16 was retrieved from the PubChem database (Compound CID: 86289587) and used as a ligand in this study. 20 different ligand poses were selected using the Lig-Prep module in Maestro v11 employing the Schrödinger platform.⁴¹ The best interaction poses were visualized using the PyMOL server (<https://pymol.org>). The most comprehensive and accurate model of ligand-protein docking and the protein function annotation was obtained from the BioLiP database (<http://zhanglab.ccmb.med.umich.edu/BioLiP/>). The free energy was minimized by the Universal Force Field and converted to the pdbqt format in PyRx0.8 for virtual screening.⁴² Furthermore, the favorable

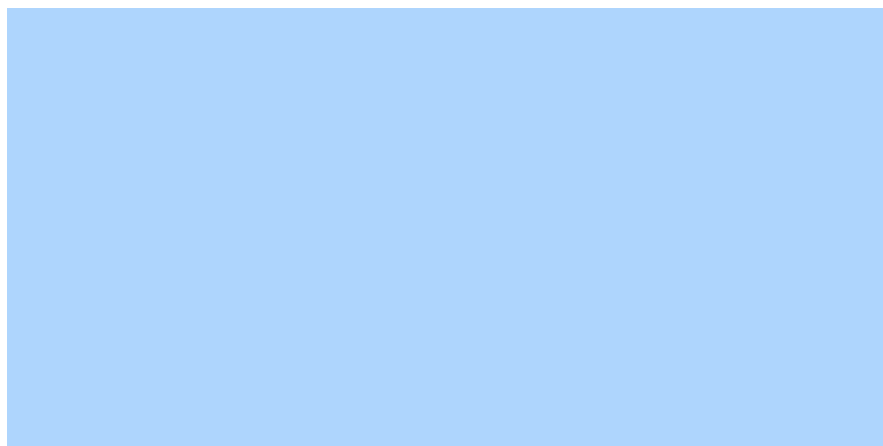
potential drug target interactions between the selected ligand molecule and modeled receptor (AdeB) were identified by the extra precision (XP) feature of Grid-based Ligand Docking with Energetics (GLIDE) in the Schrödinger platform.⁴² Each simulation was repeated three times with different initial conditions to increase the precision of the simulations and to prevent any dependencies of the results on the initial conditions. Binding sites were generated using the Site Map tool version 2.4 (Schrödinger Inc.). Finally, molecular docking was performed via AutoDock/Vina suite to assign the ligands and receptors bond orders by adding hydrogen atoms.⁴³ For docking purposes, the best docking pose was selected directly using the Glide G-Score as described previously.⁴¹ Once G-Score was obtained, it was used to build optimal binding free energy that distinguishes our sequence from the reference sequence (usually taken to be the optimal sequence). Site Map was tasked to identify the five top-ranked possible receptor suites using the default settings which include size, volume, amino acid exposure, enclosure, contact, hydrophobicity, hydrophilicity, and donor/acceptor ratio. Furthermore, the topology of the transmembrane, inside and outside α -helices was predicted by the DeepTMHMM (<https://dtu.biolib.com/DeepTMHMM>) and TOPCONS (<http://topcons.net/>) modules.

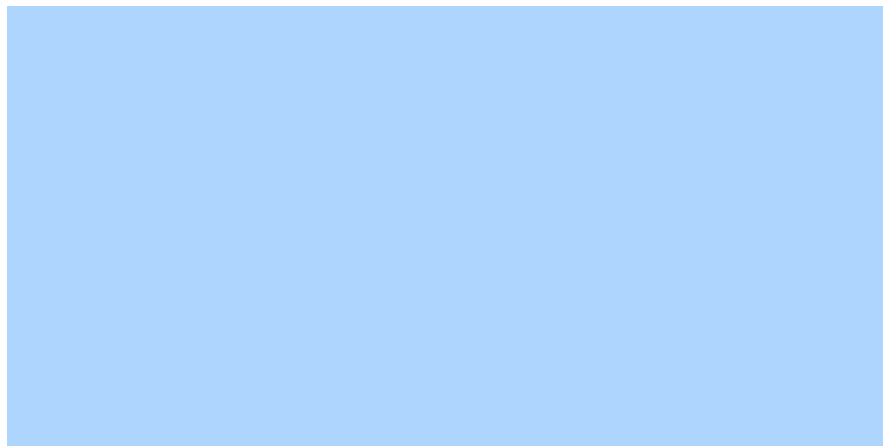
2. 9 Preparation of the contact map and domain boundaries

We predicted the AdeB protein contact map and domain boundaries using deep residual neural networks coupled with coevolutionary precision matrices (<https://zhanglab.ccmb.med.umich.edu/FUPred>). A protein contact map represents the distance between all possible amino acid residue pairs of a 3D structure. For two residues, the element of the matrix is 1 if the two residues are closer than a predetermined threshold, and 0 otherwise.⁴⁴ To achieve reliable results, we used the FUPred score for a continuous two-domain protein, using the following formula

$$FUscore2c(l) = 2N_{1,2}(l)[1N_1(l) + 1N_2(l)]$$

where l is the domain splitting point of a protein, $N_1(l)$ and $N_2(l)$ represent the number of contacts within the first and second domains, respectively, and $N_{1,2}(l) = N_{2,1}(l)$ indicates the number of contacts between the first and second domains.⁴⁵ The core idea of the algorithm was to retrieve domains boundaries locations by maximizing the number of intradomain contacts while minimizing the number of interdomain contacts from the contact map.





2. 10 Statistics

Statistical analyses were performed using SPSS 17.0 (SPSS, Chicago, IL, USA). A $p < 0.05$ was considered statistically significant for two-tailed tests.

3 RESULTS

3.1 Bacterial source and identification

In our previous reports, 65 isolates of *A. baumannii* were isolated from the ICUs hospitals in Kerman, Iran.³¹ Fifty-five of these were MDR, while 10 were carbapenems susceptible. Among them, one isolate that exhibited the highest MICs to various classes of antibiotics was selected for this study.

3.2 Antimicrobial susceptibility tests and PCR-Sequencing

The organism exhibited high MICs against gentamicin and kanamycin (64 $\mu\text{g/ml}$), ciprofloxacin and levofloxacin (125 $\mu\text{g/ml}$), ceftazidime and ceftriaxone (256 $\mu\text{g/ml}$), imipenem (125 $\mu\text{g/ml}$), colistin (8 $\mu\text{g/ml}$), piperacillin/tazobactam (125 $\mu\text{g/ml}$), and azithromycin (64 $\mu\text{g/ml}$), respectively (Figure. 1A). Furthermore, MP-B prevented the active growth of the MDR strain of *A. baumannii* with mean MIC=1 $\mu\text{g/ml}$, where 99.9% of the cell's population was not grown in Tryptic Soy broth medium ($p < 0.05$). A significant synergy was observed when the cells were grown in the presence of both antibiotics (various concentrations) and sub-MIC of MP-B (Figure 1A). The MICs against gentamicin and kanamycin were reduced to 8 $\mu\text{g/ml}$, ciprofloxacin and levofloxacin to 4 $\mu\text{g/ml}$, ceftriaxone to 2 $\mu\text{g/ml}$, carbapenems to 4 $\mu\text{g/ml}$, and tetracycline to 2 $\mu\text{g/ml}$, respectively. However, no change in the MIC level of colistin, piperacillin-tazobactam, azithromycin, co-trimoxazole, and chloramphenicol was observed (Figure. 1A). To confirm the synergism of Mastoparan-B with antibiotics, we performed growth curve analysis of the isolate in the presence and absence of sub-MIC of MP-B. When cells grown in 0.5 $\mu\text{g/ml}$ of MP-B, relatively steady growth was observed after 8 hours of incubation (Figure. 1B). The results indicated that the reduction in MIC against antibiotics was not due to the death of bacteria by Mastoparan-B but rather the inactivation of some cellular mechanism (s) such as efflux pump.

To prove this hypothesis, we performed the PCR technique by using specific primer pairs for the entire *ade B* gene. The AdeB efflux pump gene was then sequenced using Sanger's dideoxy DNA chain termination method by ABI Prism DNA Sequencer, and its expression was evaluated in the presence and absence of MP-B. Interestingly, a 20-fold decrease in the expression of the *ade B* efflux pump gene was detected when the cells were grown at the sub-MIC level of this peptide. Furthermore, we obtained the nucleotide sequence of the *ade B* gene by blasting with similar sequences in the NCBI database (<https://www.ncbi.nlm.nih.gov/blast>). From the nucleotides, we detected the AdeB protein sequence in the GenBank database.

3.3 Physicochemical parameters and Gene Ontology

The computation of physicochemical parameters of the AdeB efflux pump revealed that the protein was typically composed of 1036 amino acid residues with an average molecular weight (M. Wt.) of 112592.02 and the molar extinction coefficient of (ϵ) 81945 (Table 1A). Likewise, empirical analysis of amino acid composition by the ExPasy ProtParam database revealed the dominance of small aliphatic amino acids like alanine at 16%, isoleucine, valine at 10%, and glycine at 6.7% in the AdeB structure (Table 1B). Furthermore, documentation resources of protein families, active domains, and functional sites indicated the AdeB protein belonged to the RND transporter efflux (HAE1) similar to ArcB protein Acrflvin-R, and ACR_tran family. It showed the nonhomologous relationship with superfamily ArcB_DN_DC and pore-TolC-like domains. Gene Ontology further confirmed the biological, and functional activities of the AdeB protein. The overview of the sequence/structure diversity of the RND superfamily in this study compared to other superfamilies in the CATH database is presented in Figure. 2A. The obtained functional and structural domains by CATH were similar to MDR efflux transporter ArcB transmembrane domains with two related sequence families and one structural cluster (Figure 2A). The AdeB efflux protein had 91.8% unique sequence annotations (Figure 2B) and, the lineage had 6 functional family members in the genus *Acinetobacter* (Figure 2C).

3.4 Phylogenetic tree analysis and amino acids alignments

The phylogenetic tree analysis of the AdeB protein convincingly demonstrated high sequence identity (99.9%) with AdeB efflux pump membrane transporter tr-AOA7L9E4V2_ACIBA, tr-A0A5P6FTF2_ACIBA, and tr-A0A3Q8ULEO_ACIBA, 99.6% sequence identity with tr-AOA373B8P5.9GAMM, and 99.41% identity with efflux pump tr-A0A086HUIO_ACIBA, respectively (Figure 3A). Moreover, we also investigated blast parameters including, identity (99%), score (Average 50300), and an E-value (5.3-11) which indicated significant accuracy in clustral pattern (Figure 3B). To prove the above results, we performed multiple amino acid alignments of the AdeB and compared the amino acids helix-5 for closely related strains, the results revealed high identity among the amino acids of these strains (Figure 3C). Overall, the high identity matrix of the AdeB protein sequence was observed in the UniProtKB database ([?]99%) (Figure 3D). This indicates that a high evolutionary relationship exists among sequences in this report.

3.5 Prediction of the 3D structure of AdeB protein

The obtained AdeB trajectory showed an inner membrane protein with a 3-fold asymmetrical axis positioned perpendicular to the membrane surface with the typical RND-like folds. The predicted RND efflux pump exhibited three components; i) a 30Å U shape funnel channel in the AdeC outer membrane region composed of both α - helices and β -sheets (Figure 4A), ii) a 40 Å large periplasmic membrane fusion AdeA region with the coil-coil conformation, and iii) a 50Å transmembrane AdeB transporter helical structure in the form of helix-turn-helix with a pore (Figure 4A). The large periplasmic domain of the AdeB molecule is created by two extracellular loops that link together TM1 with TM2 and TM7 with TM8. This periplasmic domain can be divided into six subdomains, PN1, PN2, PC1, PC2, DN, and DC (Figure 4B). These features fit with the extreme variety of antibiotics recognized by AdeB. The N-terminal TM1 leads to the PN1 subdomain that connects the PN2. Similarly, TM7 leads to the PC1 subdomain that was connected to the PC2 (Figure 4B). Nevertheless, a pore connected the inner membrane cleft to the periplasmic cavity (Figure 4C). The amino acids analysis of the pore displayed a high quantity of Lys, Phe, and Ala residues (Ala residue relatively stabilized the pore channel) (Figure 4C). The combination of deep neural network learning with completed I-TASSER assembly significantly improved by threading template quality and therefore boosted the accuracy of the final model through optimized fragment assembly simulations with C-score = 1.41, TM- score =0.99, RMSD (Å) = 4.4 ± 2.9 , and P-score = 1, respectively. Nevertheless, the validity of the AdeB structure was further confirmed by the Ramachandran plot (Figure 5A) and local similarity estimate of amino acid residues in chains A, B, and C (Figure 5B). The results indicated that over 99% of the amino acid backbones remained in the Ramachandran favored regions and less in the outlier. The plot also illustrated torsional angles at low clash point ψ (0.87%) and high Ramachandran favored F (97.92%) conditions. The obtained results of the local quality estimate by the Swiss-ExPasy database for all three chains illustrated consistency in our work. Furthermore, the structural validation of the secondary protein structure using the PROSA website (Figure 5C) showed the generated model has a Z-score = 2.3, which is within the acceptable range

of -10 to 10.

3.6 Molecular docking analysis

For docking of Mastoparan-B with the AdeB protein, we prepared 20 poses and used them to determine the suitable binding site on the AdeB efflux pump. The comparison of the molecular docking simulation before and after attachment of MP-B showed MP-B attached exclusively with the helix-5 inner membrane via Val 499, Phe 454, Thr 474, Ser 461, Gly 465, and Tyr 468 residues, respectively (Figure 6A). Upon docking of the ligand, there was a change in energy minimization (glide score of 0.8 to 0.2), and a shift in the orientation of dihedral angles including phi (φ), and psi (ψ) by distances of 9.0 Å, 9.3 Å, and 9.6 Å (Figure 6B). The black arrows indicate the bond interaction potentials: bond-stretching, VB, angle-bending, VA, dihedral (out-of-plane), Vdh. The protein folding changes were detected by AlphaFold DB software. Here, we used the AlphaFold database for the first time for the determination of the AdeB domains and detailed information about folding and the position of helix-5 in the interior side of the AdeB protein (Figure 7A). In addition, the attachment of MP-B to this helix and amino acids is involved in molecular docking studied by this software represented in Figure 7B. Finally, the overall docking process, the positions of the amino acids, and H-bonds with the ligand molecule are shown in Figure 7C. Moreover, comparing the AdeB molecule with template 7cz9A as the model indicated a high score in the ligand-receptor interaction (z-score = 33.510 cutoff = 6.9).

3.5 Prediction of the position and topology of transmembrane helices

The topology of AdeB protein was predicted by both DeepTMHMM and TOPCON tools using Z-coordinates and predicted ΔG -values across the sequence and the Wilcoxon rank-sum test to get a quantified comparison between the two reliability scores independent of the overall prediction accuracy. The majority of transmembrane helices were arranged at positions between 300-500 and 900-1000. The place of binding ligand to the receptor is shown by a circle with a Z score of 5.8 (Figure 8A). Furthermore, analysis by TOPOCONS further confirmed the above results (Figure 8B), and estimated the percent of α -helix inside, membrane, and outside of the AdeB protein (Figure 8C). The transmembrane helices (TMHs) topology constituted the highest percentage in the AdeB structure. Furthermore, employing Pyr² software we determined 47.7% of amino acid residues displayed α -helical structure, 21% β - sheets, 11.5% turns, and 24.5% coil with the Z score +2.52. As a result, the most frequent topology in AdeB protein was α -helix, followed by a random coil and extended β -strand barrel.

3.8 Contact map of AdeB protein

A protein contact map represents the distance between all possible amino acid residue pairs of a three-dimensional protein structure. Here we carried out the contact map analysis of AdeB transporter by using the FUPred server. There were three overlapping D1-3, D6-2 and D6-1 at the N-terminal segment with a confidence score of 8.76 (Figure 9A). The contact maps derived from the application of a distance cutoff of 9 to 11Å around the C β atoms constitute the most accurate representation of the visualized 3D structure. Nevertheless, the domain boundaries were shown by a continuous domain curve (Figure 9B). This was followed by heat map scores which showed a low domain shift point for AdeB protein (Figure 9C). Overall, the predicted continuous domain protein secondary structure of the AdeB suggested a confidence score of >8.6, indicating our prediction was accurate.

4 DISCUSSIONS

A key part of the defense of *A. baumannii* to different antibiotics is a series of efflux pumps, which effectively exclude or reduce the intracellular concentration of a large number of antibiotics and other compounds, making the pathogen intrinsically more resistant to some antimicrobial agents.³⁰ The efflux pumps are a topic of considerable interest, both from the perspective of understanding functions and as targets for adjunct therapies.⁴⁵ In *A. baumannii*, three RND efflux systems, AdeABC, AdeFGH, and AdeIJK are reported to be primarily associated with the emergence of MDR strains.¹⁶ Other studies suggested that the AdeABC efflux pump system is the most prevalent and with the highest detection rate in clinical isolates of *A.*

baumannii as compared to other efflux pump genes.¹¹ Nevertheless, the RND efflux family in *A. baumannii* has broad substrate specificity and can efflux a vast variety of antibiotics from the periplasm before the antibiotics even fully enter the cell.⁴⁶

Despite a large number of identified efflux pumps, our understanding of the molecular mechanisms drugs effluxes remain limited and relationships between drugs and targets have been poorly understood.⁴⁷ The inhibitory mechanism between amphiphilic peptide MP-B and the AdeB efflux pump remains uncharacterized. Moreover, most of the current drug targets are proteins, and the 3D structures of these proteins need to be known in target identification.⁴⁸ Therefore, Computer-aided drug target identification methods can greatly reduce the searching scope of experimental targets and associated costs by identifying the drug binding sites and evaluating the druggability of the predicted protein.⁴⁷

The results from this study provide novel insight into the inhibitory activity of Mastoparan-B on the RND efflux pump. The preliminary susceptibility test revealed that the organism was intrinsically sensitive to MP-B as a potent inhibitor of the membrane function. However, when the cells were grown in the presence of a sub-MIC concentration of this peptide (0.5 $\mu\text{g/ml}$), and different concentrations of antibiotics, there were significant reduction in MICs particularly against aminoglycosides, fluoroquinolones, third-generation of cephalosporins, carbapenems, and tetracycline, respectively. In contrast, the MIC against colistin, piperacillin-tazobactam, azithromycin, trimethoprim-sulfamethoxazole, and chloramphenicol remained unchanged. This led us to the understanding that, the efflux pump might be involved in this extrusion of particular antibiotics but not all. The synergic activity of MP-B with antibiotics was further supported by the 20 fold decrease in transcription of the *ade B* gene in the presence of sub-MIC of MP-B. Furthermore, the search for phylogenetic analysis of AdeB protein with similar sequences in the UniProtKB database revealed a high percent identity matrix using the Maximum Likelihood method by neighbor joining method. The results indicated the AdeB that investigated in this study was evolutionary-related to the majority of Acinetobacter efflux pumps. This was further confirmed by Structural neighbourhood comparison by CATH database which showed 97.9% alignment with functional family multidrug efflux transporter AcrB transmembrane domain. The study of lineage of the protein showed six functional families with the *A. baumannii*. Structural neighbourhood of superfamily (inside superfamily) indicated evidence they have diverged from a common ancestor.

Furthermore, we performed docking of Mastoparan-B with amphiphilic α -helical structure to the inner membrane AdeB protein via the amphiphobic amino acids. By AlphaFold 2 tool, we found that, the proteins fold into a 3D dimensional shape to bury these hydrophobic side chains in the protein interior. Since there was no reliable crystallography for a membrane protein, so we rely on computational methods. These methods are based on structural, physicochemical, and evolutionary properties that distinguish binding sites from the rest of the protein surface (e.g., amino acid composition and residue conservation). Furthermore, we investigate deep learning of artificial intelligence for the prediction of the membrane topology of transmembrane proteins. The attachment of all forms of MP-B exclusively occurred to the transmembrane helix-5 which is situated at the interior of the inner membrane domain. This was confirmed by using the BioLiP database (the structure was predicted by SPARKS-X (SPX) with template 7cz9A ($z\text{-score}=33.51$ and $\text{cutoff}=6.9$). Concurrent target-ligand interaction indicated a shift in the dihedral angles with a lower free binding energy score. Furthermore, examination of the dihedral angles changes upon ligand binding showed that, the φ and ψ changes caused a transient conformational change in the protein structure resulting in the inhibition of AdeB activity. The presence of a large amount of Phe, Ala, and Lys amino acid residues in the pore region provides a hydrophobic trap around this peptide in the AdeB molecule particularly, Phe residue was important in creating this hydrophobic microenvironment. So far, the mechanisms have not been studied in detail, therefore this statement must be further confirmed. Similarly, 3 inter domain interchange was observed in AdeB α -chains by FUPred software, utilizing contact maps prediction created by deep residual neural networks coupled with coevolutionary precision matrices.

5 | CONCLUSION

AdeB is a critically important representative of the RND family of multidrug transporters in *A. baumannii*

and as such, the molecular interaction of this pump with Mastoparan-B by bioinformatics tools will provide useful new information on the targeted inhibition of efflux pumps in this bacterium. Mastoparan-B might be used in combination with antibiotics like ampicillin-sulbactam for the treatment of MDR *A. baumannii* .

AUTHORS' CONTRIBUTIONS

S.MR performed the analysis and participated in the design of the study, OZ, and OT, helped in writing and correcting of paper, FM helped drafted the manuscript and analysis of data, and G.MM help with software collection and information analysis. All authors read and approved the final manuscript

DATA AVAILABILITY STATEMENT

The authors confirm that the data supporting the findings of this study are available within the article and its supplementary materials.

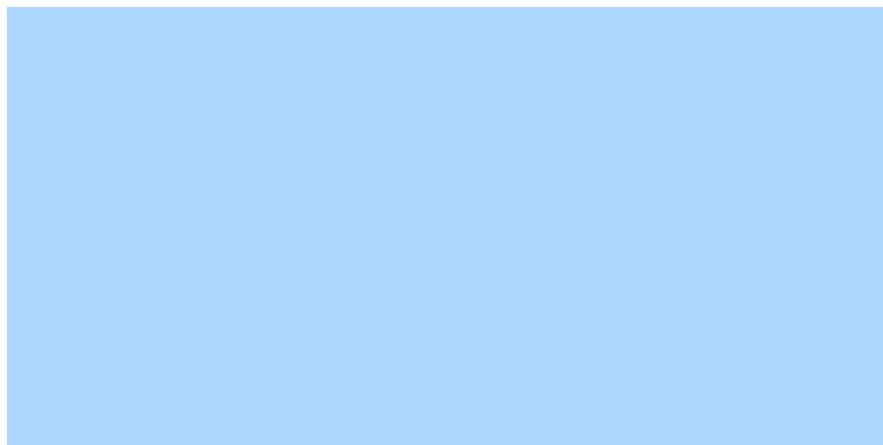
CONFLICTING INTERESTS

The authors declare that they have no competing interests.

FUNDING

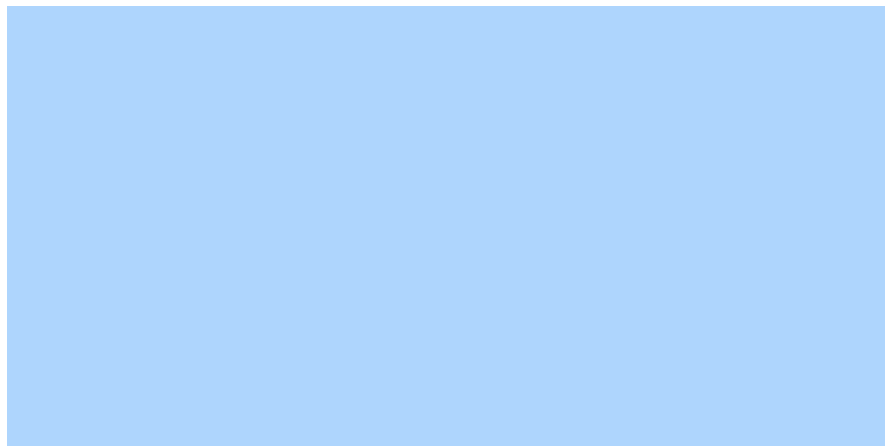
Not applicable.

ORCID



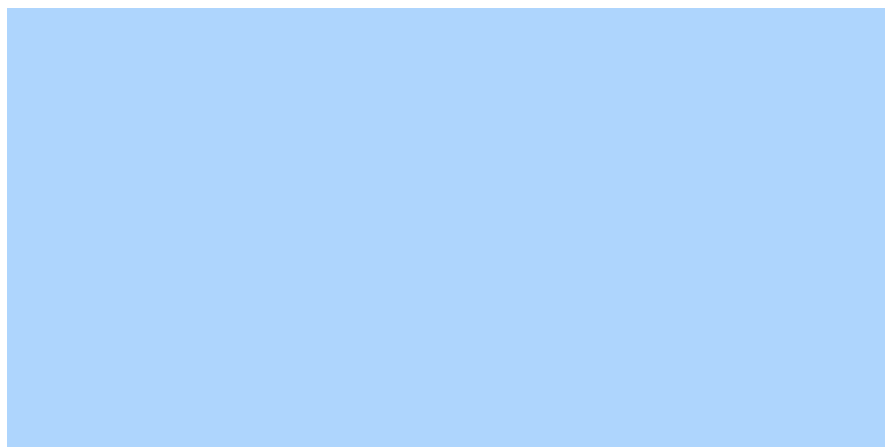
Mohammad Reza Shakibaie

<https://orcid.org/0000-0003-2524-125X>



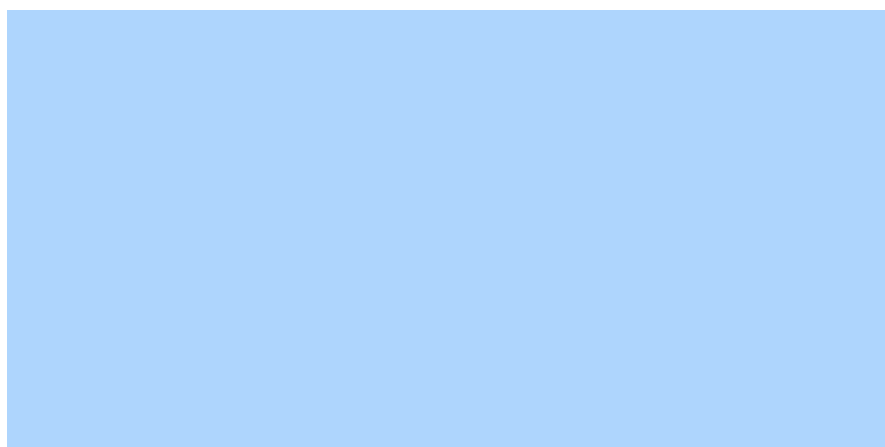
Farzan Modaresi

<https://orcid.org/0000-0001-6253-7629>



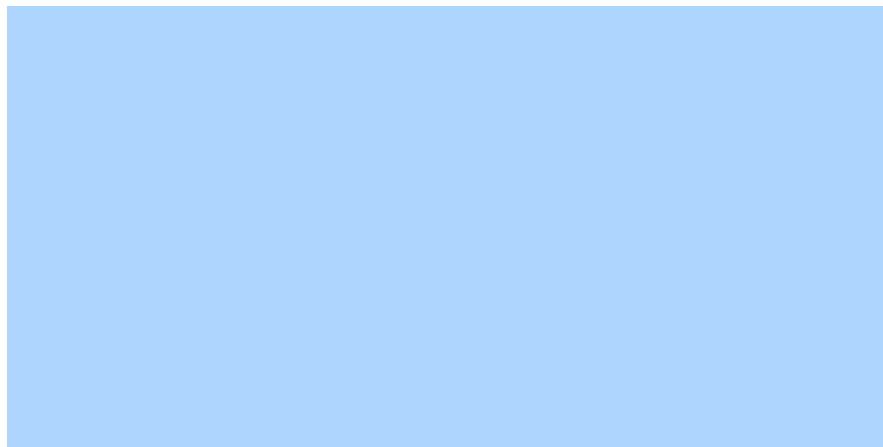
Omid Azizi

<https://orcid.org/0000-0001-7759-8029>



Omid Tadjrobehkar

<https://orcid.org/0000-0002-5562-8070>.



Mohammad Mehdi Ghaemi

<https://orcid.org/0000-0001-6427-2740>

REFERENCES

1. Lin X, Li X, Lin X. A review on applications of computational methods in drug screening and design. *Molecules* . 2020; 25(6):375.
2. Shoichet BK. Virtual screening of chemical libraries. *Nature* . 2004; 432(7019):862-5.
3. Forli S, Huey R, Pique ME, Sanner M.F, Goodsell DS, Olson AJ. Computational protein-ligand docking and virtual drug screening with the AutoDock suite. *Nat Protoc* . 2016;11(5):905–919.
4. Jumper J, Evans R, Pritzel A, et al. Highly accurate protein structure prediction with AlphaFold. *Nature*. 2021; 596:583–589.
5. Shakibaie MR, Adeli S, Salehi MH. Antibiotic resistance patterns and extended-spectrum β -lactamase production among *Acinetobacter* spp. isolated from an intensive care unit of a hospital in Kerman, Iran. *Antimicrob Resist Infect Control* . 2012;1:1.
6. Tacconelli E, Carrara E, Savoldi A, et al. The WHO priority list of antibiotic-resistant bacteria and tuberculosis. *Lancet Infect Dis* . 2018;18(3):318-327.
7. Asif M, Alvi IA, Rehman SU. Insight into *Acinetobacter baumannii* : pathogenesis, global resistance, mechanisms, treatment options, and alternative modalities. *Infect Drug Resist* . 2018;11:1249-1260.
8. Paulsen IT. Multidrug efflux pumps and resistance: regulation and evolution. *Curr Opin Microbiol* . 2003;6(5):446– 451.
9. Kakoullis L, Papachristodoulou E, Chra P, et al. Mechanisms of antibiotic resistance in important Gram-Positive and Gram-Negative pathogens and novel antibiotic solutions. *Antibiotics* . 2021;10(4):415.
10. Bastian-Tashkan B, Niakan M, et al. Antibiotic resistance assessment of *Acinetobacter baumannii* isolates from Tehran hospitals due to the presence of efflux pumps encoding genes (*ade A* and *ade S* genes) by molecular method. *BMC Res Notes* . 2020;13(1):543.
11. Abdi SN, Ghotaslou R, Ganbarov K, et al. *Acinetobacter baumannii* efflux pumps and antibiotic resistance. *Infect Drug Resist* . 2020;13:423-434.

12. Coyne S, Courvalin P, Perichon B. Efflux-mediated antibiotic resistance in *Acinetobacter* spp. *Antimicrob Agents Chemother* . 2011; 55(3):947-53.
13. Du D, Wang-Kan X, Neuberger A, et al. Multidrug efflux pumps: structure, function, and regulation. *Nat Rev Microbiol*.2018;16(9):523-539.
14. Ornik-Cha A, Wilhelm J, Kobylka, J, et al. Structural and functional analysis of the promiscuous AcrB and AdeB efflux pumps suggests different drug binding mechanisms. *Nat Commun*. 2021;12(1):6919.
15. Magnet S, Courvalin P, & Lambert T. Resistance-nodulation-cell division-type efflux pump involved in aminoglycoside resistance in *Acinetobacter baumannii* strain BM4454. *Antimicrob Agents and Chemother*. 2001;45(12): 3375–3380.
16. Alav I, Kobylka J, Kuth MS, et al. Structure, assembly, and function of tripartite efflux and type 1 secretion systems in Gram-Negative bacteria. *Chem Rev*. 2021;121(9):5479-5596.
17. Yoon EJ, Balloy V, Fiette L, Chignard M, et al. Contribution of the Ade resistance–nodulation–cell division–type efflux pumps to fitness and pathogenesis of *Acinetobacter baumannii*. *MBio*.2016;7 e00697-16.
18. Leus IV, Weeks JW, Bonifay V, et al. Substrate specificities and efflux efficiencies of RND efflux pumps of *Acinetobacter baumannii*. *J Bacteriol*. 2018; 200(13):e00049-18.
19. Yu EW, Aires JR, McDermott G, Nikaido H. A periplasmic drug-binding site of the AcrB multidrug efflux pump: a crystallographic and site-directed mutagenesis study. *J Bacteriol*. 2005;187(19):6804-15.
20. Su CC, Morgan CE, Kambakam S, et al. Cryo-Electron Microscopy structure of an *Acinetobacter baumannii* multidrug efflux pump. *mBio*. 2019;10(4):e01295-19.
21. Carpenter EP, Beis K, Cameron AD, et al. Overcoming the challenges of membrane protein crystallography. *Curr Opin Struct Biol*.2008;18(5):581–586.
22. Krogh A, Larsson B, von Heijne G, et al. Predicting transmembrane protein topology with a hidden markov model: application to complete genomes. *JMB*; 305(3): 567-580.
23. Käll L, Rogh A, Sonnhammer EL. A combined transmembrane topology and signal peptide prediction method. *J Mol Biol*. 2004;338(5):1027-36.
24. Bernsel A, Viklund H, Hennerdal A, Elofsson A. TOPCONS: consensus prediction of membrane protein topology. *Nucleic Acids Res*. 2009; 37(2):W465–W468
25. Terreni, M, Taccani, M, & Pregnolato, M. New antibiotics for multidrug-resistant bacterial strains: latest research developments and future perspectives. *Molecules*. 2021;26(9): 2671.
26. Lin CH, Cheng T, Lin Shyu C, et al. Structural and biological characterization of mastoparans in the venom of *Vespa* species in Taiwan. *Peptides*. 2011;32(10):2027-2036.
27. Epand RM, Vogel HJ. Diversity of antimicrobial peptides and their mechanisms of action. *Biochim Biophys Acta*. 1999;15;462(1-2):11-28.
28. Sato H, Feix JB. Peptide–membrane interactions and mechanisms of membrane destruction by amphipathic α -helical antimicrobial peptides. *Biochimica et Biophysica Acta (BBA)*. 2006;1758(9):1245-56.
29. Wang Y, Venter H, Ma S. A novel approach to combat efflux-mediated drug resistance in bacteria. *Curr Drug Targets*. 2016;17(6):702-19.
30. Jamshidi S, Sutton JM, and Khondaker MR. Computational study reveals the molecular mechanism of the Interaction between the efflux inhibitor PA β N and the AdeB transporter from *Acinetobacter baumannii*. *ACS Omega*. 2017;2(6):3002-3016.
31. Skariyachan S, Manjunath M, Bachapanavar N. Screening of potential lead molecules against prioritized targets of multidrug-resistant *Acinetobacter baumannii* insights from molecular docking, molecular dynamic simulations, and in vitro assays. *J Biomol Struct Dyn*. 2019;37(5):1146-1169.
32. Modarresi F, Azizi O, Shakibaie MR, et al. Effect of iron on the expression of efflux pump (adeABC) and quorum sensing (*luxI*,*luxR*) genes in clinical isolates of *Acinetobacter baumannii*. *APMIS* 2015;123(11): 959–968.
33. CLSI. Clinical and laboratory standards institute. Document No M100S. Performance Standards for Antimicrobial Susceptibility Testing. 26. Wayne: CLSI; 2019.
34. Masoumi S, Shakibaie MR, Gholamrezazadeh M, Monirzadeh F. Evaluation Synergistic Effect of TiO₂, ZnO nanoparticles and amphiphilic peptides (Mastoparan-b, Indolicidin) against drug-resistant *Pseudomonas aeruginosa*, *Klebsiella pneumoniae* and *Acinetobacter baumannii*. *Arch Pediatr Infect Dis*. 2018;6(3):e57920.
35. Livak KJ, Schmittgen TD. Analysis of relative gene expression data using real-time quantitative PCR and the 2(-Delta Delta C(T)). *Methods* . 2001; 25(4):402-8.
36. Azizi O, Shakibaie MR, Badmasti F, et al. Class 1 integrons in non-clonal multidrug-resistant *Acinetobacter baumannii* from Iran, description of the new blaIMP-55 allele in In1243. *J Med Microbiol*. 2016; 65(9):928-936.
37. Stamatakis A, Hoover P, Rougemont J. A rapid bootstrap algorithm for the RAxML

Web servers. *Syst Biol.* 2008;57(5):758-71.

38. Wiederstein M, Sippl MJ. ProSA-web: interactive web service for the recognition of errors in three-dimensional structures of proteins. *Nucleic Acids Res.* 2007; 35: W407-10.

39. Benkert P, Künzli M, Schwede T. QMEAN server for protein model quality estimation. *Nucleic Acids Res.* 2009;37(Web Server issue):W510-4. 40. Hooft RW, Sander C, Vriend G. Objectively judging the quality of a protein structure from a Ramachandran plot. *Comput Appl Biosci.* 1997;13(4): 425-430. 41. Ganeshan S, Shakibaie MR, Rajagopal R. Insights from the molecular docking analysis of colistin with the PmrA protein model from *Acinetobacter baumannii*. *Bioinformatics.* 2022; 18:41-49. 42. Tripathi SK, Muttineni R, Singh SK. Extra precision docking, free energy calculation, and molecular dynamics simulation studies of CDK2 inhibitors. *Theoretical Biol.* 2013; 334:87-100. 43. Trott O, and Olson, AJ. AutoDock Vina: improving the speed and accuracy of docking with a new scoring function, efficient optimization, and multithreading. *J Comput Chem.* 2010;31(2):455-461. 44. Zheng W, Zhou X, Wuyun Q, Pearce R, Li Y, Zhang Y. FUPred: detecting protein domains through deep-learning-based contact map prediction. *Bioinformatics.* 2020; 36(12):3749-3757. 45. Dreier J, Ruggerone P. Interaction of antibacterial compounds with RND efflux pumps in *Pseudomonas aeruginosa*. *Front Microbiol.* 2015;6:660. 46. Subhadra B, Oh MN, and Choi CH. RND efflux pump systems in *Acinetobacter*, with special emphasis on their role in quorum sensing. *J Bacteriol Virol.* 2019;49:1-11. 47. Kunihiko N, Seiji Y, Ryosuke N, Martijn Z, Mitsuko HN. Function and inhibitory mechanisms of multidrug efflux pumps. *Front in Microbiol.* 2021;12: DOI. 10.3389/fmicb.2021.737288. 48. Liao, J.; Wang, Q.; Wu, F; Huang, Z. In Silico Methods for Identification of Potential Active Sites of Therapeutic Targets. *Molecules.* 2022, 27, 7103.

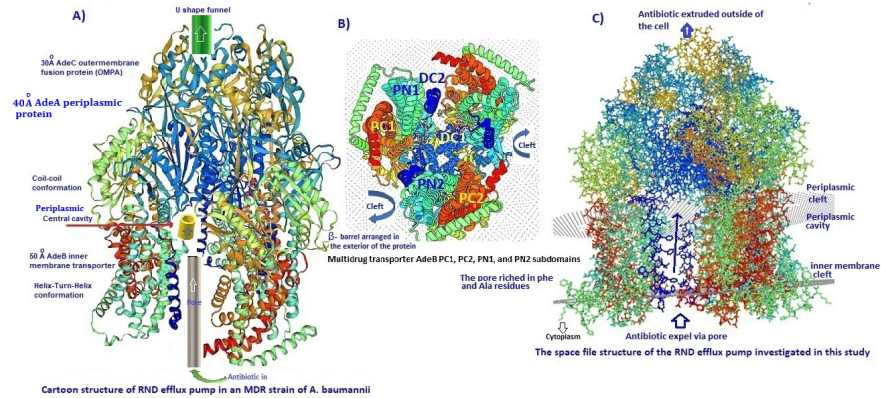
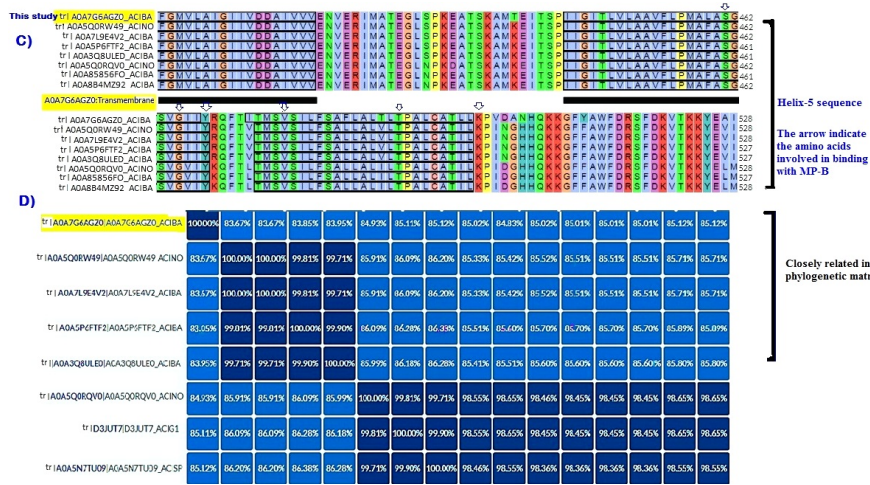
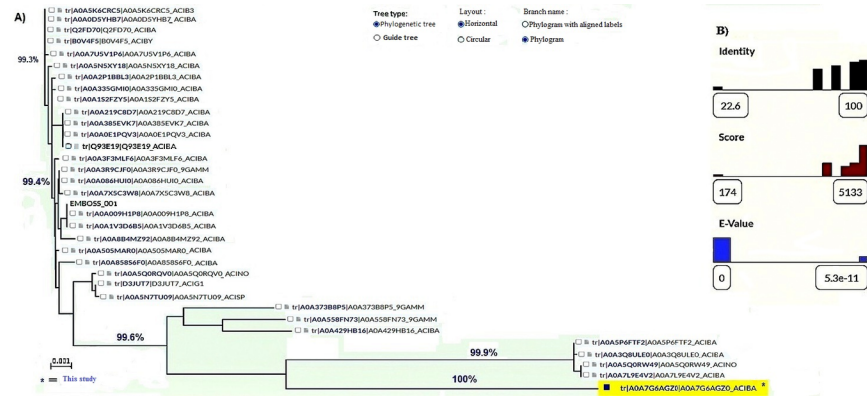
Figures legends

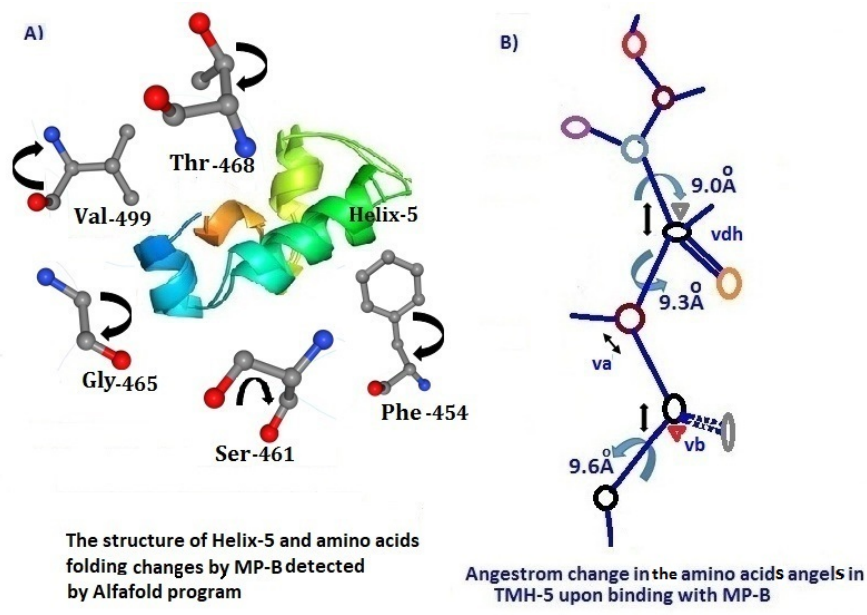
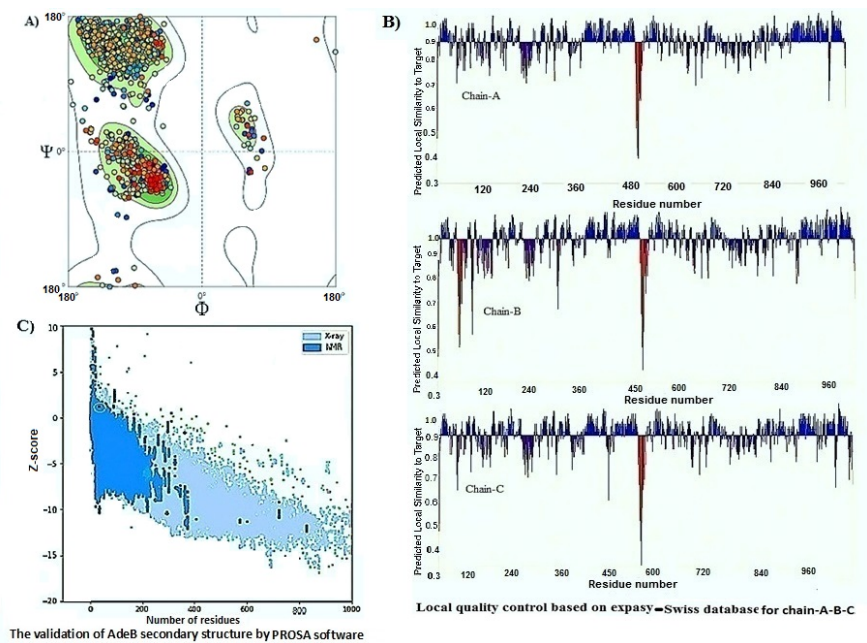
Figure. 1. A) Antibiotic susceptibility of a multidrug-resistant *A. baumannii* isolates against 12 antibiotics in the presence and absence of sub-MIC concentration (0.5 $\mu\text{g/ml}$) of Mastoparan-B. The experiment was performed by broth microdilution test as described by CLSI -2019. **B)** Growth curve analysis of an *A. baumannii* isolate in the presence and absence of sub-MIC of MP-B. Values are presented as mean \pm SD of three independent tests.

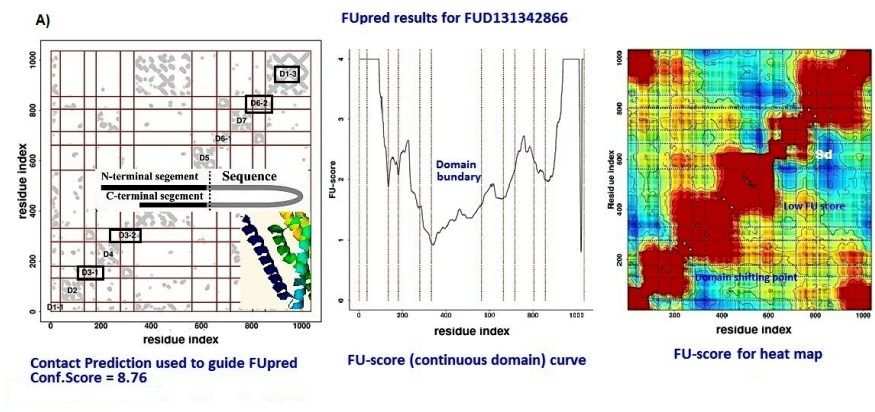
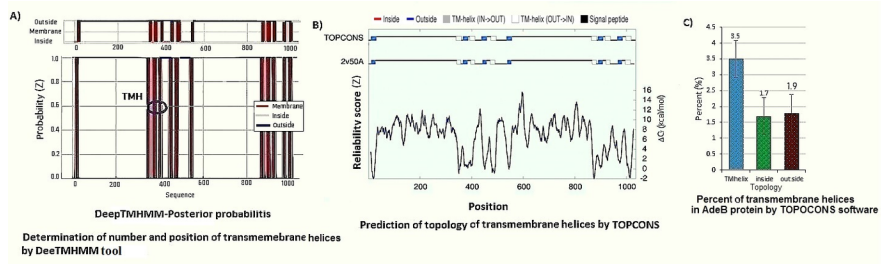
Figure. 2. A) Overview of the sequence/structure diversity of the RND superfamily compared to other superfamilies in CATH (Class Architecture Topology Homologous superfamily). The data indicated that close superfamily relation among RND efflux pump using MDR efflux pump ArcB. The red color circle indicate the position of our family **B)** Unique species annotations and diversity by CATH showed 91.8% similarity among RND family, **C)** comparing the lineage of superfamily of ArcB indicated at least 6 lineage identity with *A. baumannii* .

Figure. 3. A) Phylogenetic tree evaluation of AdeB protein using UniProtKB database. For the phylogeny study we use multiple amino acids alignment program and compared the sequences among AdeB from different *Acinetobacter* sp. The percent identity was calculated by determination of e-value from each sequence, **B)** AdeB sequence parameters including Identity, Score, and E-value of AdeB. **C)** Multiple amino acid alignment of helix-5 of AdeB protein with closely related AdeB sequences in UniProtKB, **D)** Percent identity matrix among closest sequences (SD<99.4%).

Figure. 4. Schematic of representative structures of RND multidrug transporters and tripartite assemblies. **A)** Cartoon structural prediction of the AdeABC RND efflux pump; a 30Å AdeC protein containing α/β barrel associated with a funnel and H⁺ antiporter fusion (OMPA) activity extrude antibiotic outside the cells. A 40 AdeA periplasmic protein with a heavy coil structure in the form of coil-coil conformation, the AdeA was associated with a large periplasmic cavity. A 50 the AdeB multidrug efflux pump inner membrane protein. The AdeB inner transmembrane helix contained a long narrow pore that connected to the central cavity. **B)** The distal end of AdeB contains PC1, PN1, PC2, and PN2 subdomains with three clefts. **C)** The wireframe diagram of the AdeABC RND efflux pump system shows the AdeB as an inner transmembrane helix, a narrow pore (rich in Phe, Lys, and Ala residues), a central cavity, a periplasmic fusion protein (OMPA), and 3 chains ABC associated with RND component. The docking site was shown by a circle.







Hosted file

Table.docx available at <https://authorea.com/users/567780/articles/613951-conformational-changes-in-the-adeb-transmembrane-efflux-pump-by-amphiphilic-peptide-mastoparan-b-down-regulates-expression-of-the-ade-b-gene-and-restores-antibiotics-susceptibility>